COMPUTATIONAL AERO-ACOUSTICS OF VEHICLE A-PILLAR AT VARIOUS WINDSHIELD RADII

Nurul M. MURAD[1], Jamal NASER[1], Firoz ALAM[2] and Simon WATKINS[2]

[1] Faculty of Engineering and Industrial Science

Swinburne University of Technology, VIC, 3122 AUSTRALIA

[2] School of Aerospace, Mechanical and Manufacturing Engineering

RMIT University, VIC, 3083 AUSTRALIA

ABSTRACT

Flow separation behind the A-pillar region can lead to aero-acoustics generation, which presents problems such as annoyance and discomfort to vehicle occupants (Hucho, 1998). The propagation of aerodynamic noise surrounding the vehicle can be modelled numerically in order to investigate the aero-acoustics source and hence minimise the problems. This paper attempts to investigate one of the several methods available to model aero-acoustics propagation. In this paper, three generic vehicle scale models with different windshield radii were used as a case study and modelled using CAA under laboratory operating conditions. CAA modelling was conducted using a commercial code called AVL SWIFT-CAA. AVL SWIFT-CAA offered a more economical avenue to model for CAA. Investigations were carried out at inlet velocity of 60, 100 and 140km/h at 0° and 15° yaw angles. Comparisons were conducted between CAA results and experimental results of Alam (2000) to investigate the capabilities of the SWIFT-CAA modelling capabilities.

NOMENCLATURE

CFD   Computational Fluid Dynamics
CAA Computational Aero-Acoustics
RANS   Reynolds Average Navier Stokes Equations
LEE   Linearized Euler Equations
C_p *RMS*   Root Mean Square Coefficient of Pressure
PSD   Power Spectral Density

INTRODUCTION

Flow separation behind the vehicle A-pillar region can lead to aero-acoustics generation. Aero-acoustics generated is then transferred to the passenger cabin causing annoyance and much discomfort to the vehicle occupants (Hucho, 1998).

The propagation of aerodynamic noise surrounding the exterior and interior of the vehicle can be modelled numerically. One method of aero-acoustics modelling is to use either DNS or LES CFD modelling. The performance of these methods however, is limited by the spatial and temporal resolution that can be achieved in order to effectively model the required frequency and amplitude range, Tam (2002), Lokhande et al. (2003).

The other method of aero-acoustics modelling involve extracting acoustical source term from either a transient or steady CFD model and calculate the propagation of aerodynamic noise at the far-field receiver using an acoustic solver. Lyrintzis (1994) and Kumarasamy et al. (1999) defined this method as the acoustic-analogy method and listed several of the different techniques available, namely the Lighthill Acoustic Analogy (LAA) Method, Kirchoff Method, Pertubation Method and the Linearised Euler Equation (LEE) Method.

This purpose of this paper is to investigate the capability of a CAA modelling code called the hybrid SWIFT-CAA, developed by AVL/TNO. The hybrid SWIFT-CAA approach offers a novel way to economically model aero-acoustics by using RANS-CFD data coupled with a statistical model as a basis to solve for the acoustical source term. This bypass the need to generate a transient CFD model that utilises a computational domain with high order spatial and temporal resolution needed to solve for aero-acoustics propagation that extends to the far field range.

The capabilities of the hybrid SWIFT-CAA was investigated through comparison with the experimental work of Alam (2000), in which measurement of C_p RMS and PSD distribution behind the vehicle A-pillar region were obtained. Alam (2000) used three generic vehicle scale models with different circular windshield radii and yaw orientations, subjected to various wind tunnel velocities.

The following section will describe the methodology used in this study. This includes the general description of the hybrid SWIFT-CAA approach and the strategy used for the CAA modelling. The results and discussion are then presented through comparison of C_p RMS and PSD results distribution at 0° and 15° yaw between the experimental and CAA modelling approach of surface acoustic fluctuating pressure behind the model A-pillar region.

METHODOLOGY

The methodology of the hybrid SWIFT-CAA approach can be categorised into two steps. The first step consists of generation of acoustical source term by mean of transferring 3D statistical turbulent quantities obtained from RANS-CFD modelling to a separate CAA domain, meshed with unstructured tetrahedral grid of low density. The transfer of 3D statistical turbulent quantities (turbulent kinetic energy, eddy length scale and dissipation rate) were conducted using a statistical model that incorporate the inverse Fourier transform through a sub-routine in the CAA solver, called the Unstructured Kinematic Source Generator (UKSG). The statistical model developed by Bechera (1996) and Longatte (1998) are given as:

$$\overline{u}_t(x,t) = 2\sum_{n=1}^{N} \tilde{u}_n \cos\left(\kappa_n x + \psi_n + \omega_n t\right)\sigma_n \quad (1)$$

where σ_n is the direction of turbulent velocity vector, which is perpendicular to κ_n the wave vector. ω_n is the radial frequency, ψ_n was a random phase and $\tilde{u}_n$ is the model amplitude, which contains the statistical turbulent quantities obtained from the RANS-CFD modelling.

The equation for turbulent fluctuations is then used to determine a time accurate acoustic source term for the perturbation term of the mass, momentum and energy equation:

$$\frac{\partial \rho_a}{\partial t} + \vec{\nabla}.\left(\rho_o \vec{u}_a + \rho_a \vec{U}_o\right) = S'_M - S_{A1} \quad (2)$$

$$\frac{\partial u_a}{\partial t} + \left(\vec{U}_o.\vec{\nabla}\right)\vec{u}_a + \left(\vec{u}_a.\vec{\nabla}\right)\vec{U}_o$$
$$-\frac{\rho_a}{\rho_o^2}(\vec{\nabla}p_o) + \frac{p_a}{\rho_o^2}\left(\vec{\nabla}\rho_o\right) = S_I - S_{A2} \quad (3)$$

$$\frac{\partial p_a}{\partial t} + \vec{\nabla}.\left(\vec{U}_o p_a + \gamma \vec{u}_a p_o\right) - (\gamma-1)\vec{u}_a.\vec{\nabla}p_o$$
$$+ (\gamma-1)p_a\vec{\nabla}.\vec{U}_o = S'_E - S_{A3} \quad (4)$$

which represents the source terms with subscripts A1 to A3 in equation 2 to 4.

The final step in the SWIFT-CAA approach was to determine the aero-acoustics propagation (source to receiver in the far-field) through solving for the acoustic pressure (p_a). Using the acoustic source terms, the CAA solver determine the aero-acoustics propagation using the LEE approach, which involves conversion of the terms on the right hand side of equation 2 to 4, together with a time domain calculation conducted using a Quadrature Free Discontinuous Galerkin Spatial discretization approach. In this approach, the revised source term obtained progressively at each time interval from the UKSG subroutine was interpolated to the CAA solver. A new time step interval was then obtained through the use of a fourth-order Runge-Kutta algorithm, AVL (2003).

Vehicle Geometry and Boundary Conditions

The geometry configurations and boundary conditions used in the CFD modelling, prior to the CAA modelling were obtained from Alam (2000). Generic scale (40%) vehicle models with varying local windshield radii namely Small Ellipsoidal (299-mm elliptic radius), Semi Circular (374-mm) and Large Ellipsoidal (449-mm) were constructed at yaw angle orientations of 0˚, -15˚ and +15˚ respectively. The models were exposed to wind tunnel inlet velocities of 60, 100 and 140-km/h. The windshield for the models was at a slant angle of 60˚ from the vertical axis (Figure 1).

The external surface of the CAA volume domain was assigned boundary conditions of either reflecting (wall of the CAA domain) or non-reflecting (inlet and outlet of the CAA domain) (Figure 2). In the CAA domain, two rows (bottom and top row) of monitoring locations (96-mm apart) were assigned to each model to capture fluctuating pressures behind the A-pillar region. Each row had 16 monitoring points, which were 32.0-mm apart (Figure 1).
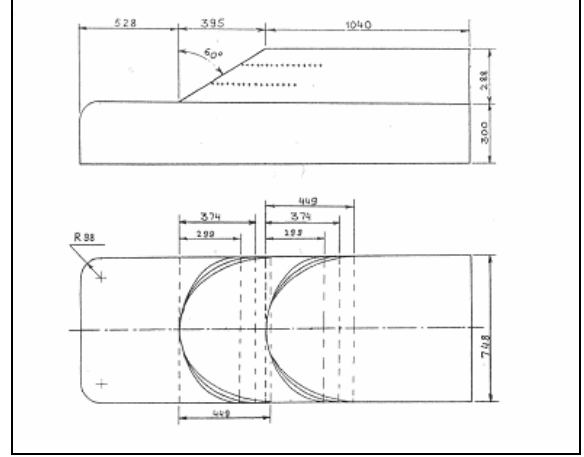
Figure 1: Simplified Vehicle Model Geometry with Varying A-pillar Windshield Radius (After Alam, 2000)
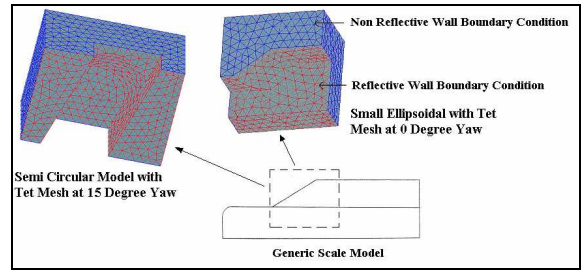
Figure 2: Unstructured Tetrahedral Grids in CAA Domain Mesh Generation

AVL Fame Hybrid was used to generate grids for the CAA domain. The CAA domain was created by first selecting an area of interest surrounding the A-pilar region from within the CFD domain. The surrounding surface of the selected CAA domain was first meshed with triangulate surface grids. The CAA domain volume was then meshed with unstructured tetrahedral grids (Figure 2). Each grid cell in the CAA domain must adhere to an aspect ratio of smaller than 3.3 in order to maintain optimum accuracy. Each tetrahedral grids generated varies in between 50-mm to 100-mm in size.

The final total grid count generated varies in between 14,000 to 35,000 depending on the model radius configuration and yaw angle orientation.

Numerical Scheme and Strategy

The RANS-CFD modelling conducted using SWIFT-CFD used a turbulence intensity and length scale value of 1.8% and 5.8 mm (1.0% model height) respectively. The numerical scheme used during the initial stage of calculation was first order upwind scheme and central differencing scheme. Once convergence was reached, the AVL smart bound higher order scheme was then used. The convergence level for residuals was set to 0.1% with SIMPLE pressure-velocity coupling used together with 3D, steady and incompressible flow environment. Turbulence models used in the initial calculation was standard k-ε before switching to the Reynolds Stress turbulence model (RSM). More details of the RANS-CFD modelling conducted using SWIFT-CFD are well documented in Murad (2006) and will not be discussed further in this paper.

For CAA modelling conducted using SWIFT-CAA, a CAA Mapper sub-routine was first used to map the 3D statistical turbulence quantities obtained from the CFD results to the CAA domain. The CAA Mapper divided the CAA domain into several rectangular partitions or bins to expedite the mapping and interpolation process. The amount of CFD nodes interpolated in each bin must be sufficiently high to ensure an accurate mapping. In this study, the node interpolation value was set as ten, the recommended default value. Once the mapping and interpolation process was complete, the CAA Mapper was then able to establish an initial time step to be used in the CAA solver. The initial time step was given automatically and was based on the formulation that utilises the mean velocity together with the grid size and the Courant number.

The time interval generated for the CAA solver varies between 3.0 to 16.0 microseconds and required 160,000 to 270,000 time steps to complete a total of 1.0-second time interval propagation.

In setting up the CAA solver to simulate for the aerodynamic acoustic propagation, the input parameters for Turbulence Realization Sampling Frequency was assigned a value of 40-kHz, which was the maximum allowed. This was close to the value of 48-kHz, which was used by Alam (2000).

For this study, the simulation of the acoustic propagation carried out by the CAA solver took between one to four days to finish. Calculation of the CAA solver for this project was done using a single processor in the Swinburne University Super Computer cluster.

The results were analysed using post-processing features available in SWIFT-CAA. PSD analysis were conducted by providing input such as the number of Fourier Fast Transform (FFT) blocks, Number of FFT overlap points and viewing Window for each Fourier block. For this study, the inputs used were as follows:

- Number of FFT blocks – 4096
- Number of FFT overlap points – 50%
- Viewing Window for each block – Hanning

COMPARISON AND DISCUSSION OF CAA AND EXPERIMENTAL RESULTS

CAA Modelling Results of Surface Fluctuating Pressure

Small Ellipsoidal Model, C_p RMS and PSD Results

Comparison of C_p RMS distribution obtained from CAA and experimental results for Small Ellipsoidal model at 0˚, -15˚ (Leeward) and +15˚ (Windward) yaw can be seen in Figures 3, 4 and 5. Good correlations were obtained for both bottom and top row monitoring locations at 0˚ and +15˚ yaw. However, a small C_p RMS discrepancy of around 0.05 exists at -15˚ yaw towards the halfway point of the bottom row monitoring locations and towards the end of the top row monitoring locations respectively.

Comparison of PSD distribution between CAA model and experimental results for Small Ellipsoidal model at 100 km/h can be seen in Figures 6 and 7. The discrepancies obtained for peak PSD values for 0˚ yaw, +15˚ and -15˚yaw were 1.0, 3.0 and 14.0 dB respectively. The overall PSD distribution for Small Ellipsoidal model showed best correlation at yaw angle of +15˚, followed by yaw angles of 0˚ and -15˚, with total mean discrepancies measured at 5.0, 7.3 and 13.3-dB respectively.
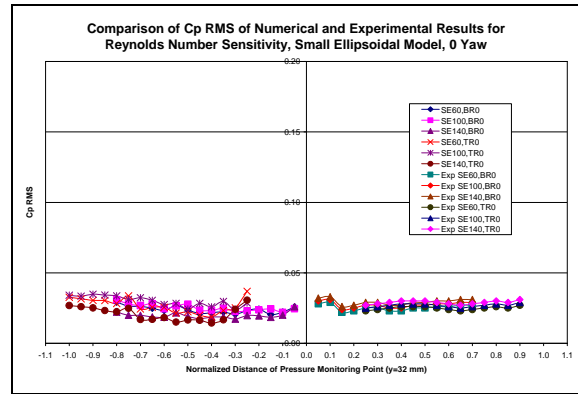

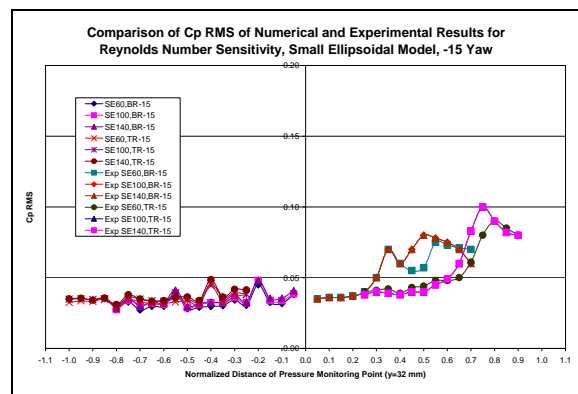**Figure 3**: C_p RMS for Small Ellipsoidal Model at 0˚ Yaw

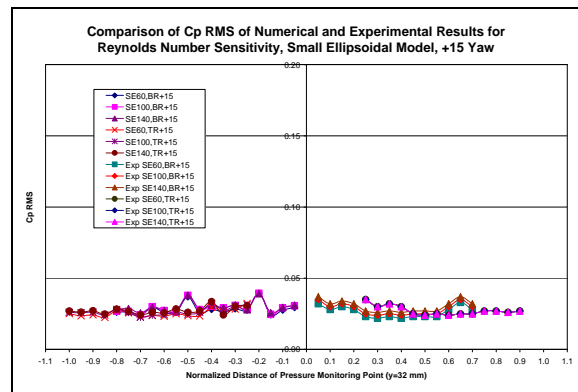**Figure 4**: C_p RMS for Small Ellipsoidal Model at -15˚ Yaw

Figure 5: C_p RMS for Small Ellipsoidal Model at +15˚ Yaw

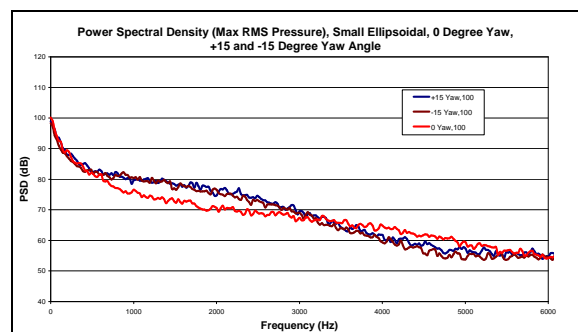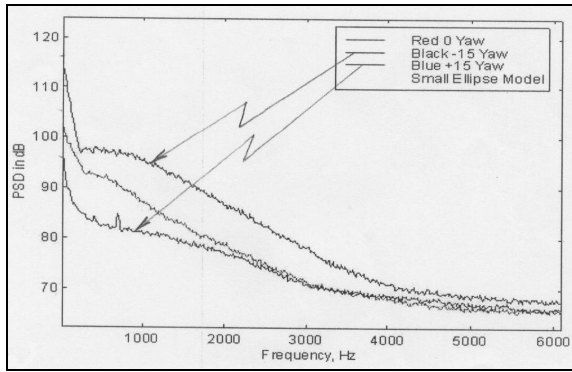**Figure 6**: CAA Modelling of Spectral Energy Density Distribution for Small Ellipsoidal Model at -15˚, 0˚ and +15˚ Yaw

Figure 7: Experimental Results of Spectral Energy Density Distribution for Small Ellipsoidal Model at -15˚, 0˚ and +15˚ Yaw (After Alam, 2000)Semi Circular Model, C_p RMS and PSD Results

Comparison of C_p RMS distribution obtained from CAA and experimental results for Semi Circular model at 0˚ yaw yield good correlations for both the bottom and top row monitoring locations. However, comparison of C_p RMS distribution between CAA and experimental results showed slight discrepancy at both -15˚ and +15˚ yaw orientation, particularly towards the rear portion of the bottom and top row monitoring points with values of around 0.05 and 0.02 respectively (Figures 8, 9 and 10).
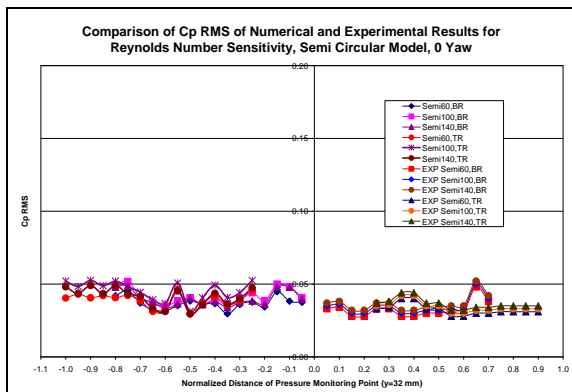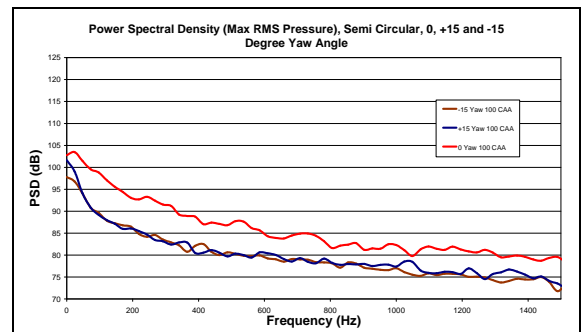

Figure 8: C_p RMS for Semi Circular Model at 0˚ Yaw
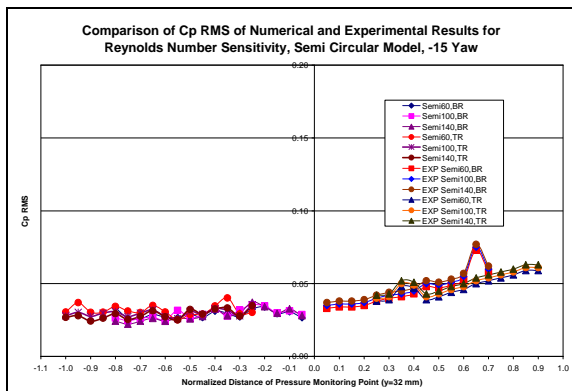
Figure 9: C_p RMS for Semi Circular Model at -15˚ Yaw

Comparison of peak PSD values between CAA and experimental results at 100 km/h yielded lowest discrepancy at 0˚ yaw, followed by -15˚ and +15˚ yaw, measuring 14.0, 18.0 and 19-dB respectively. The overall PSD distribution discrepancy obtained for Semi Circular
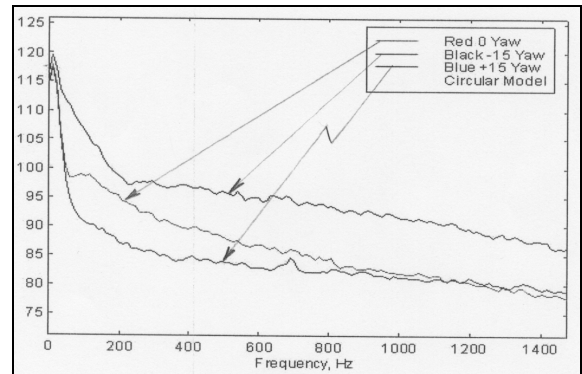
model was 7.0, 12.0 and 15.0-dB, corresponding to yaw angles at 0˚, +15˚ and -15˚ respectively (Figures 11 and 12).
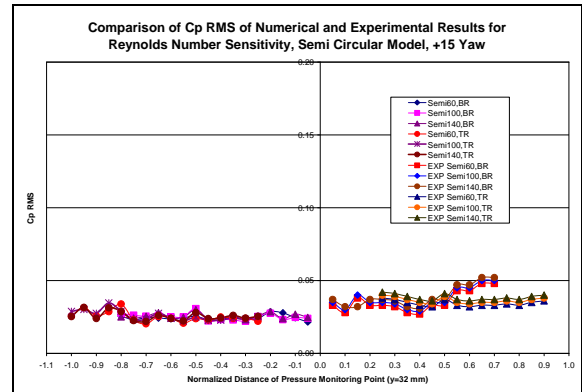
Figure 10: C_p RMS for Semi Circular Model at +15˚ Yaw

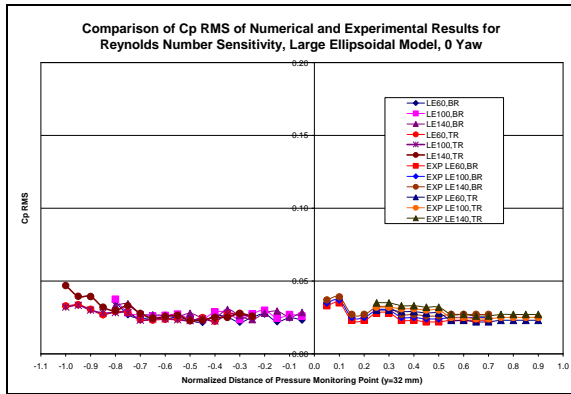**Figure 11**: CAA Modelling of Spectral Energy Density Distribution for Semi Circular Model at -15˚, 0˚ and +15˚ Yaw

Figure 12: Experimental Results of Spectral Energy Density Distribution for Semi Circular Model at -15˚, 0˚

Large Ellipsoidal Model, C_p RMS and PSD Results

Comparison C_p RMS distribution obtained from CAA and experimental results for Large Ellipsoidal model at 0˚and -15º and +15˚ yaw yield good correlations for both the bottom and top row monitoring locations with discrepancy of C_p RMS observed at values less than 0.02 (Figures 13, 14 and 15).

Comparison of peak PSD values obtained from CAA and experimental results at 100 km/h produced discrepancies of 5.0, 13.0 and 15.0-dB, corresponding to yaw angles at 0º, -15˚ and +15˚ respectively. The overall PSD discrepancies for Large Ellipsoidal was the lowest at 0˚ yaw, followed by yaw angles at -15˚ and +15˚, measuring 3.0, 6.8 and 10.0-dB respectively (Figures 16 and 17).

4
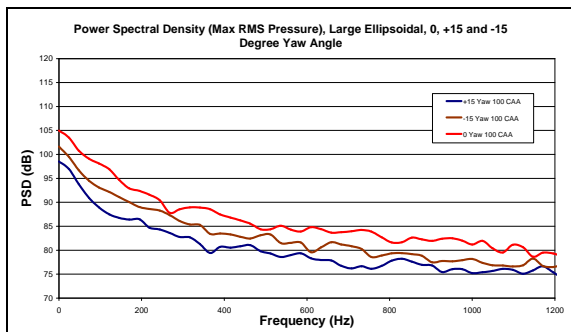
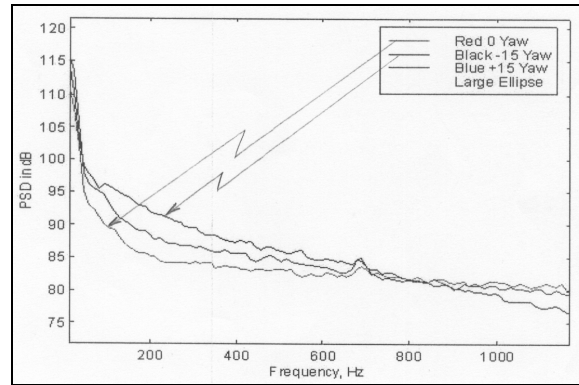**Figure 13:** C_p RMS for Large Ellipsoidal Model at 0° Yaw
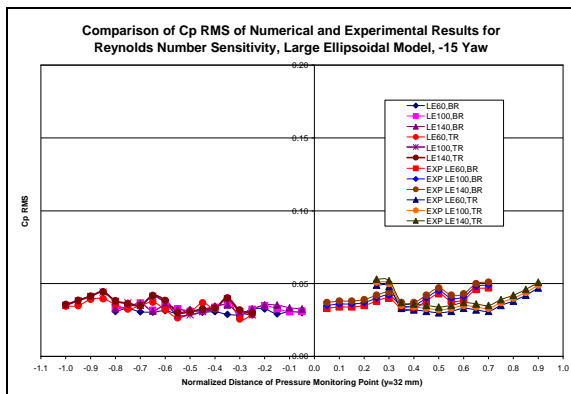
Figure 14: C_p RMS for Large Ellipsoidal Model at -15° Yaw Capabilities of SWIFT-CAA in modelling for Fluctuating Surface
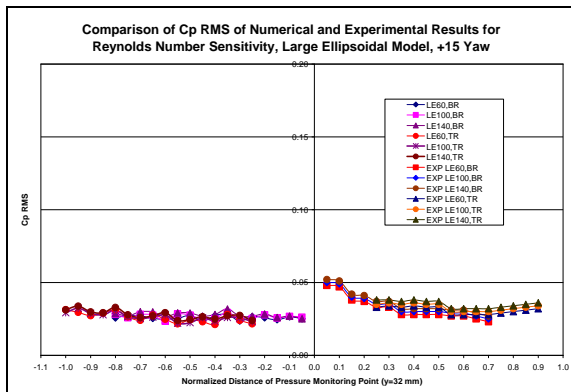
Figure 15: C_p RMS for Large Ellipsoidal Model at +15° Yaw

Figure 16: CAA Modelling of Spectral Energy Density Distribution for Large Ellipsoidal Model at -15°, 0° and +15° Yaw

Figure 17: Experimental Results of Spectral Energy Density Distribution for Large Ellipsoidal Model at -15°, 0° and +15° Yaw (After Alam, 2000)

The study of Alam (2000) showed that aerodynamic properties behind the A-pillar region for models with variable windshield radii were a mixture of attached and separated flow with aerodynamic noise generation caused largely by the presence of intense turbulence boundary layer distributed underneath the flow. SWIFT-CAA provided good correlation against results obtained experimentally in modelling for the C_p RMS distribution behind the A-pillar region, particularly for model positioned at 0° yaw and +15° yaw.

However, a maximum discrepancy of 0.05 was displayed when predicting the Cp RMS at -15° yaw. This was due to the generation of small scale separation as the flow moves downstream to the rear region of the monitoring location, which was a direct consequence to the leeward yawing angle of the model.

The discrepancies caused in modelling for the C_p RMS provided a direct implication in the outcome of the PSD distribution. The comparison of results obtained showed under prediction of PSD distribution by the CAA modelling. A maximum discrepancy of around 0.02 obtained from the C_p RMS distribution translates to a maximum mean PSD discrepancy of around 10-dB. A maximum discrepancy of around 0.05 translates to a maximum mean PSD discrepancy of around 15-dB. Comparison done on literature review based on CAA modelling behind a bluff body region showed similar discrepancies, Lokhande et al. (2003), Ogawa et al. (1999), Strumolo et al. (1998), Uchida et al. (1999).

Contour visualisation of the acoustic pressure propagation and overall sound pressure level (OASPL) distribution can be seen in Figures 18, 19 and 20. Despite the under prediction showed by the quantitative results obtained from the CAA modelling, the presence of turbulence boundary layer intensity and small scale separation was still captured through the contour visualisation.

CONCLUSION

In summary, this study has shown that the AVL SWIFT-CAA has good CAA modelling capabilities in predicting the aeroacoustics propagation behind the A-pillar region of scale models with variable windshield radii and yawing angle. The maximum discrepancies of 0.05 and 15-dB for predicting C_p RMS and PSD distribution obtained from using AVL SWIFT-CAA were comparable to similar studies of CAA modelling. In addition, important aero-
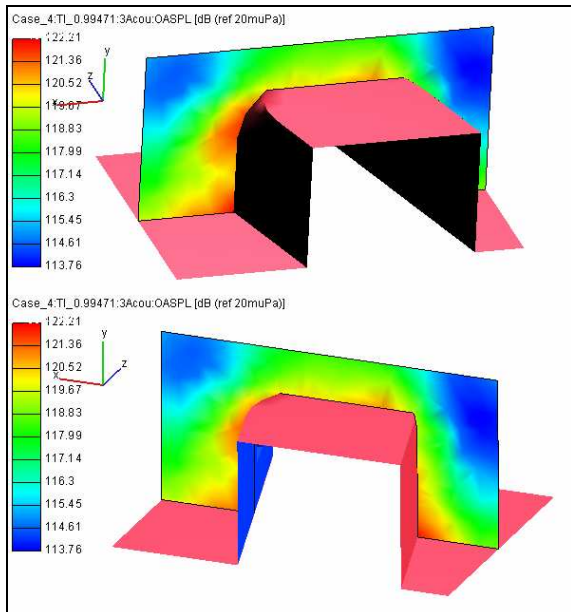
acoustics characteristics were captured through the visualisation of acoustic pressure and OASPL contours.
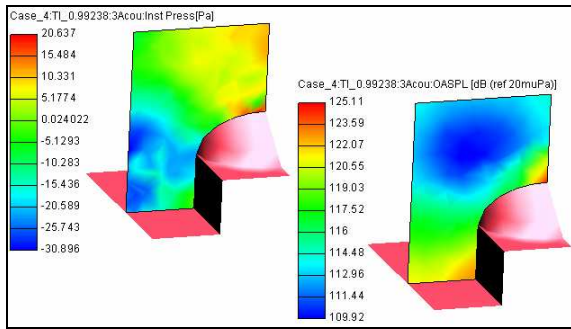
Figure 18: Acoustic Pressure Propagation, Small Ellipsoidal Model at 0˚ Yaw
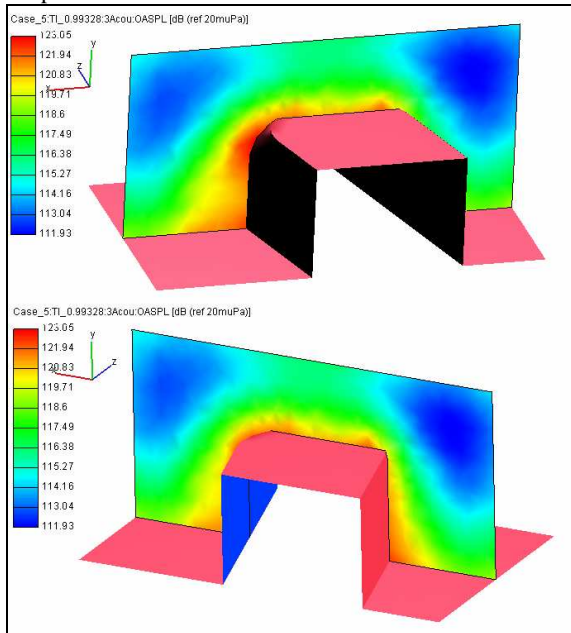
Figure 19: Overall SPL Distribution, Small Ellipsoidal Model at 15˚ Yaw

Figure 20: Overall SPL Distribution, Semi Circular Model at 15˚ Yaw

REFERENCES

ALAM, F., (2000), "The Effects of Car A-Pillar and Windshield Geometry and Yaw Angles on Local Flow and Noise: PhD Thesis", RMIT University, Australia.

AVL SWIFT, (2003), "AVL User Manual", Ver. 3.1, Austria.

BECHERA, W., LAFON, P., BAILLY, C. and CANDEL, S. (1996), "Application of a k-ε Turbulence Model to the Prediction of Noise from Simple and Co-axial Free Jets", *J. Sound and Vibr.,* **97**, No. 6, 3518-3531.

GEORGE, A.R., (1990), "Automobile Aerodynamic Noise", *SAE Paper*, No 900315.

HUCHO, W.H. ed., (1998), "Aerodynamics of Road Vehicles", 2nd edn, Butterworths, London.

KUMARASAMY, S. and KARBON, K. (1999), "Aeroacoustics of an Automobile A-Pillar Rain Gutter: Computational and Experimental Study", SAE Paper, No 1999-01-1128.

LOKHANDE, B., SOVANI, S. and XU, J. (2003), "Computational Aeroacoustics Analysis of a Generic Side View Mirror", SAE Paper, No 2003-01-1698.

LONGATTE, E., (1998), "Modélisation de la propagation et de la génération du bruit au sein des écoulements turbulents internes", These présentée pour l'obtention du Docorat de l'Ecole Central Paris.

LYRINTZIS, A.S. (1993), "The use of Kirchoff's Method in Computational Aeroacoustics", Computational Aero and Hydro-Acoustics, ASME.

MURAD, N.M., NASER, J., ALAM, F. and WATKINS, S., (2002), "CFD Modelling of Vehicle A-Pillar Aerodynamics", *Proceedings of the Second International Conference on Computational Fluid Dynamics*, Sydney Australia, July 15-19.

MURAD, N.M. (Complete in 2006), "Computational Fluid Dynamics of Vehicle Aerodynamics and Associated Acoustics: PhD Thesis", Swinburne University, Australia.

OGAWA, S. and KAMIOKA, T. (1999), "Review of Aerodynamic Noise Prediction Using CFD", SAE Paper, No 1999-01-1126.

STRUMOLO, G., BABU, V. and TOMAICH, T. (1998), "A Lattice-Based Analysis of Vehicle Aerodynamic Noise", *WUA-CFD 4th World Conference and Exhibition in Applied Fluid Dynamics*, Freiburg Germany, June 1998.

TAM, C.K.W. (2002), "Computational Aeroacoustics: An Overview", *10th Annual Conference of the CFD Society of Canada*, Windsor ON, Canada, June 9-11 2002.

UCHIDA, K. and OKUMURA, K. (1999), "Aerodynamic Noise Simulation based on Lattice Boltzmann Method (Surface Pressure Fluctuations around A-pillar)", SAE Paper, No 1999-01-1127. and +15˚ Yaw (After Alam, 2000)